Journal of Geophysical Research: Oceans

RESEARCH ARTICLE
10.1029/2017JC013639

Sustenance of Phytoplankton in the Subpolar North Atlantic During Winter

Farid Karimpour[1], **Amit Tandon**[1], **and Amala Mahadevan**[2]

[1]Department of Mechanical Engineering, University of Massachusetts Dartmouth, Darthmouth, MA, USA, [2]Woods Hole Oceanographic Institution, Woods Hole, MA, USA

Key Points:
- Fronts reduce the depth of the mixed layer in winter by restratifying it
- Phytoplankton growth is enhanced in the presence of fronts in winter, compared to the case without fronts
- Highly variable air-sea fluxes have little effect on the phytoplankton growth in the subpolar North Atlantic during winter

Correspondence to:
F. Karimpour,
fkarimpour@umassd.edu

Citation:
Karimpour, F., Tandon, A., & Mahadevan, A. (2018). Sustenance of phytoplankton in the subpolar North Atlantic during winter. *Journal of Geophysical Research: Oceans*, *123*, 6531–6548. https://doi.org/10.1029/2017JC013639

Received 17 NOV 2017
Accepted 23 MAY 2018
Accepted article online 12 JUN 2018
Published online 14 SEP 2018

Abstract We consider two factors that affect the mixed layer depth (MLD) and potentially contribute to phytoplankton sustenance over winter—variability of air-sea fluxes and three-dimensional processes arising from horizontal density gradients (fronts). The role of these two factors is addressed using several three-dimensional idealized numerical simulations in a process study ocean model forced with air-sea fluxes at different temporal averaging frequencies. Results show that in winter, when the average mixed layer is much deeper than the euphotic layer and the period of daylight is short, phytoplankton production is relatively insensitive to high-frequency variability in air-sea fluxes. Short-lived stratification events during light-limited conditions have very little impact on phytoplankton production. On the other hand, the slumping of fronts shallows the mixed layer in a patchy manner and the associated restratification persists considerably longer than that caused by changes in air-sea fluxes. Simulations with fronts show that in winter, the average MLD is about 600 m shallower than simulations without fronts. Prior to spring warming, the depth-integrated phytoplankton concentration in the model with fronts is about twice as large as the case without fronts. Hence, even in winter, restratification by fronts is important for setting the MLD; it increases the residence time of phytoplankton in the euphotic layer and contributes to phytoplankton growth, thereby sustaining phytoplankton populations in winter. Higher model resolution intensifies submesoscale dynamics, leading to stronger restratification, shallower mixed layers, greater variability in the MLD, and more production of phytoplankton.

1. Introduction

Phytoplankton are one of the lowest end members of the food web in the ocean and hence have a first-order effect on sustaining life in aquatic environments. Like plants, phytoplankton rely on photosynthesis to fix carbon and produce oxygen, but unlike plants that are fixed, they are adrift and are substantially affected by ocean currents (see Mahadevan, 2016 for a recent review). In general, the consumption of dissolved inorganic carbon by phytoplankton in the sunlit ocean allows more carbon dioxide, a key greenhouse gas, to be dissolved in the ocean from the atmosphere. Therefore, phytoplankton can have a substantial impact on the ecosystem and contribute to the oceanic uptake of CO_2 from the atmosphere (Takahashi et al., 2009). The North Atlantic, well-known for its springtime phytoplankton bloom, is one of the biologically active regions of the ocean that is responsible for about 25% of the net uptake of anthropogenic CO_2 from the atmosphere. (Sabine et al., 2004; Takahashi et al., 2009).

Productivity of phytoplankton is controlled by different mechanisms (Miller & Wheeler, 2012), including availability of light and nutrients. During winter, nutrients are replete in the ocean (Townsend et al., 1994) and phytoplankton production is limited by the low-level sunlight of short winter days (Sverdrup, 1953). Strong cooling and wind forcing cause the upper ocean surface to actively mix to a few hundred meters, creating a deep oceanic mixed layer (ML). The induced turbulent, convective motions deprive phytoplankton of the limited sunlight at the surface during winter in the subpolar North Atlantic. Therefore, it is important to know what physical mechanisms help sustain the phytoplankton population through winter, which sets the initial conditions for the rapid, exponential growth and bloom of phytoplankton in the early spring (D'Asaro, 2008).

Different scenarios contributing to the sustenance of phytoplankton have been proposed. Riley et al. (1949) derived a relationship between the turbulence and sinking velocity without considering the light dependence of phytoplankton. Sverdrup (1953) proposed the well-known critical depth hypothesis, arguing that there is a net growth of phytoplankton when the mixed layer depth (MLD) is shallower than a critical depth. Sverdrup's

model assumes that the mixed layer is well mixed and nutrients are abundant. The suitability of his proposition has become a matter of debate, as other researchers such as Behrenfeld (2010) and Boss and Behrenfeld (2010) observed growth in deep winter mixed layers deeper than the critical depth. Behrenfeld (2010) used the dilution-recoupling hypothesis and discussed that the deepening of mixed layer decreases the grazing pressure, which consequently increases the phytoplankton population. Huisman et al. (1999, 2002) argued that phytoplankton can survive when there is an intermediate level of turbulence in the water column. They introduced a maximal (critical) and minimal turbulence level for the production of phytoplankton, arguing that below the critical turbulence level, phytoplankton growth overcomes turbulent mixing. But a minimum level of turbulence is required to overcome sinking and retain phytoplankton in the euphotic layer. Later, Backhaus et al. (2003) and D'Asaro (2008) discussed that the scenario presented by Huisman et al. (1999, 2002) is incomplete as the convection caused by cooling of the ocean surface during winter is not incorporated. They argued that orbital motions in the so-called convective mixed layer (CML) enable phytoplankton to be transported from depth to the euphotic layer (and vice versa) and hence can potentially sustain growth. Therefore, convection creates a virtual euphotic layer, deeper than the actual euphotic layer, in which the phytoplankton production is sustained. More recently, Taylor and Ferrari (2011a) discussed that the shutdown of convection reduces turbulent mixing and allows phytoplankton to grow before the spring warming. Brody and Lozier (2010) evaluated the bloom by developing a mixing length scale based on buoyancy forcing and wind stress. They concluded that the bloom begins when the mixing length scale is shallower than euphotic layer. They challenged the suggestions that link increase in phytoplankton to shutdown of ocean surface cooling (Taylor & Ferrari, 2011a), as increase in chlorophyll was observed while the ocean surface was still cooling. Moreover, although turbulent mixing and MLD are reduced with weaker winds, no significant relationship was seen with the local wind speed and chlorophyll rates of change.

The hypotheses mentioned above provide reasonable explanations of how one-dimensional processes affect phytoplankton; however, an investigation of the interplay between phytoplankton productivity and three-dimensional processes coupled with air-sea fluxes is still needed. Fronts are ubiquitous in the real ocean and are sources of several forms of instabilities and three-dimensional processes, which can result in increased vertical stratification. While winter conditions are generally harsh in the subpolar ocean, periods of reduced wind stress and increased heat flux have been observed in the subpolar North Atlantic (Lacour et al., 2017). In a recent study, Lacour et al. (2017) investigated blooms during winter in the subpolar North Atlantic and found that regions of shallow MLD (i.e., MLD $<$ 100 m), formed by mixed layer eddies arising from fronts, are very common in the ocean during winter. Patchy stratification is associated with varying levels of vertical mixing and light exposure for phytoplankton. The light level in the stratified shallow patches is considerably higher than deep regions, which leads to increased phytoplankton growth in about 70% of the stratified regions.

The mixed layer is sustained through a competition between processes that increase the turbulent mixing and processes that restratify the mixed layer (Mahadevan et al., 2010). Air-sea fluxes have a first-order effect on the turbulence and mixed layer (Plueddemann et al., 1995). While convective fluxes due to cooling, evaporation, or down-front winds push heavier water over lighter water, increase turbulent mixing, destroy the stratification, and deepen the mixed layer, heating, fresh water, and up-front winds can regenerate the stratification of the mixed layer. The modulation of turbulent mixing and stratification by air-sea fluxes will eventually affect phytoplankton production. Strong winter storms and surface cooling intensify turbulent mixing, deepen the ML and decrease phytoplankton concentration. On the contrary, physical processes that increase the stratification or shoal the MLD, such as warming events and up-front winds, increase the residence time of phytoplankton in the euphotic layer.

Both mesoscale eddies (McGillicuddy, 2016), as well as three-dimensional submesoscale processes associated with frontal instabilities on length scales $\mathcal{O}$(0.1 – 10 km) and time scales of a few days (Boccaletti et al., 2007; Fox-Kemper et al., 2008; Mahadevan et al., 2012) contribute to the production and distribution of phytoplankton. Phytoplankton growth time scales are on the order of days and hence can get influenced by three-dimensional submesoscale instabilities (Mahadevan et al., 2012; Taylor & Ferrari, 2011b; Whitt et al., 2017), but the ensuing vertical restratification cannot be captured in models that rely on one-dimensional budgets for prediction of the MLD. The mixed layer is maintained through surface fluxes, vertical mixing, and both lateral and vertical processes, which need to be investigated through three-dimensional numerical simulations that are able to properly resolve submesoscale processes.

Using three-dimensional numerical simulations, we aim to answer three main questions regarding phytoplankton production and sustenance in the subpolar North Atlantic during winter in the presence of fronts and forced by realistic high-frequency air-sea fluxes: (1) Do episodic, high-frequency air-sea fluxes influence phytoplankton productivity? Intermittency in surface forcing (weakening in the heat loss, wind strength, or change in wind orientation relative to local front direction) can lead to short-lived periods of localized stratification that can potentially support weak phytoplankton blooms by creating pockets of near-surface stratification where phytoplankton can acquire enough light for transient growth. The next bout of strong cooling or down-front winds will mix phytoplankton. We aim to explore whether the recurrent ephemeral stratification and phytoplankton growth, interspersed by mixing events, can help to maintain a seed phytoplankton population through winter. (2) How do fronts contribute to sustenance of phytoplankton in winter? This is an important question considering the proven role of fronts in stratification and since winter is an active season for submesoscale processes (Callies et al., 2015; Luo et al., 2016). (3) What is the effect of numerical model resolution on predicting the MLD and phytoplankton abundance in winter?

In order to answer these questions we simulate the dynamics of the subpolar North Atlantic upper ocean in winter, under the influence of highly variable air-sea fluxes and stratifying submesoscale eddies arising from fronts. We perform highly resolved three-dimensional numerical simulations that can capture submesoscale instabilities using the Process Study Ocean Model (PSOM; Mahadevan, 2006). The model is similar to Mahadevan et al. (2012) in its setup and initialization but is located at 50°N, where there is some light for photosynthesis in winter and forced by high-frequency (hourly) wintertime air-sea fluxes based on reanalysis data. The k-ϵ turbulence closure scheme is used to account for mixing. In this article, we evaluate upper ocean physical-biological interactions in the model and address questions related to sustenance of phytoplankton in the turbulent ocean during winter. In section 2, we discuss the problem setup and numerical approach. The model findings on the role of air-sea fluxes and frontal instabilities for sustaining phytoplankton in winter are presented in section 3. Finally, in section 4, we conclude by reviewing the important role of three-dimensional frontal processes on the primary productivity in winter.

2. Numerical Simulations

2.1. Numerical Model and Turbulence Closure Scheme

We use the PSOM (Mahadevan, 2006), a three-dimensional model that solves the Reynolds-averaged Navier-Stokes momentum and tracer equations. The Reynolds decomposition and averaging of the fluid flow governing equations lead to extra subgrid-scale turbulent momentum fluxes ($\overline{u_i' u_j'}$) and turbulent scalar fluxes ($\overline{u_i' c'}$), which cannot be solved directly and are parameterized in the numerical model (Pope, 2000). Here i and $j = 1, 2$, and 3 represent x, y, and z directions, $\overline{(\,)}$ denotes the spatial or temporal average, and u' and c' are turbulent velocity and turbulent scalar fields, respectively. For subgrid-scale fluxes, PSOM is coupled with the General Ocean Turbulence Model developed by Burchard et al. (1999) to benefit from more sophisticated turbulence closure schemes, such as the k-ϵ turbulence model (Jones & Launder, 1972) or K Profile Parameterization (KPP) model (Large et al., 1994) in our simulations.

PSOM solves the discretized Reynolds-averaged Navier-Stokes equations while relying on General Ocean Turbulence Model for the calculation of the turbulent fluxes. We use the standard k-ϵ closure scheme (Jones & Launder, 1972) and the turbulent viscosity hypothesis to link the turbulent momentum fluxes to the mean gradient of the velocity as

$$\overline{u_i' u_j'} = -K_{ij}^m \bar{S}_{ij}, \tag{1}$$

where K_{ij}^m is the turbulent (eddy) viscosity and $\bar{S}_{ij} = 1/2\left(\partial \bar{U}_i/\partial x_j + \partial \bar{U}_j/\partial x_i\right)$ is the mean strain rate. In the k-ϵ closure scheme the vertical turbulent viscosity (K_z^m) is calculated as a function of the turbulent kinetic energy (k) and the dissipation rate of the turbulent kinetic energy (ϵ) as

$$K_z^m = C_\mu \frac{k^2}{\epsilon}, \tag{2}$$

where $C_\mu = 0.09$. In this model, k and ϵ are obtained by solving separate evolution equations that incorporate advection terms, the effect of production and destruction of turbulence, buoyancy forces, and inhomogeneity arising from the solid boundary (e.g., bottom of the ocean; Karimpour & Venayagamoorthy, 2014). This model parameterizes three-dimensional turbulent processes and incorporates the effects of highly variable air-sea fluxes and buoyancy forces.

To calculate the mixing of the tracer (i.e., density, heat, and salinity), PSOM uses the gradient-diffusion hypothesis, which assumes that the turbulent scalar fluxes are transported down the mean scalar gradient and are calculated as

$$\overline{u_j' c'} = -K_j^d \frac{\partial \bar{C}}{\partial x_j}, \tag{3}$$

where K_j^d is the turbulent diffusivity.

We assume that the horizontal turbulent viscosity and diffusivity are isotropic (i.e., invariant under rotation), equal, and constant as $K_x^m = K_y^m = K_x^d = K_y^d = 0.1$ m^2/s. The vertical turbulent viscosity (K_z^m) is calculated through equation (2) and the turbulent diffusivity is calculated as $K_z^d = K_z^m / Pr_t$, where Pr_t is the turbulent Prandtl number, which is the linking bridge between the turbulent viscosity and diffusivity (Karimpour & Venayagamoorthy, 2014). We use the Pr_t parameterization proposed by Venayagamoorthy and Stretch (2010), formulated as follows

$$Pr_t = \frac{Ri_g}{R_{f\infty}} + Pr_{t0}\left(-\frac{Ri_g}{Pr_{t0}\Gamma_\infty}\right). \tag{4}$$

Here $Ri_g = N^2/S^2$ is the gradient Richardson number, N is the buoyancy frequency, and S is the horizontal mean velocity gradient (i.e., mean shear rate) in the vertical direction. R_f is the flux Richardson number and $R_{f\infty} = 0.25$ and $\Gamma_\infty = 1/3$ are the flux Richardson number and the mixing efficiency when $Ri_g \to \infty$. Also, $Pr_{t0} = 0.7$ is the neutral turbulent Prandtl number, where there is no density stratification.

2.2. Domain Description

We use a three-dimensional model domain that is 96 km × 480 km × 1,000 m, in x (or zonal), y (or meridional), and z (or vertical) directions respectively, with $n_x = 96$, $n_y = 480$, and $n_z = 48$ grid cells in the zonal, meridional, and vertical directions. We use a horizontal resolution of $\Delta x = \Delta y = 1{,}000$ m to allow resolving submesoscale processes and a stretched grid in the vertical direction with resolution ranging from about 2.5 m at the surface to 48 m at the bottom of the domain. The zonal direction uses periodic boundary conditions, while in the meridional direction the boundaries are solid walls. The model uses a time step of 432 s to evolve the momentum and scalar evolution equations. An approximate location of the modeled domain in the subpolar North Atlantic is shown in Figure 1a. The blue box on the right corner of Figure 1a shows the location of the North Atlantic Bloom Experiment (NAB08), which was conducted in April–June 2008 to study the spring bloom to the south of Iceland (Fennel et al., 2011). Figure 1b shows the schematic of the modeled domain. The chosen location (50°N) for our simulations in the North Atlantic has complex dynamics, involving strong currents and mesoscale eddies (Rossby, 1996). In this idealized process study, however, we aim to isolate the effects of submesoscale fronts and variability in air-sea fluxes on phytoplankton productivity in wintertime, in a light-limited region of the subpolar North Atlantic, represented in our simulations by the location 50°N. The more southern location of 50°N in this study, compared to NAB08, allows for winter phytoplankton production.

2.3. Atmospheric Forcing

The numerical model is forced by National Aeronautics and Space Administration's Modern-Era Retrospective analysis for Research and Applications, Version 2 (MERRA-2) data for 2008. MERRA-2 is a satellite-based reanalysis data set produced with the Global Modeling Assimilation Model Office/Goddard Earth Observing System Model, Version 5 (GMAO/GEOS-5) data assimilation system (Bosilovich et al., 2015). The model is forced with hourly MERRA-2 fluxes spatially averaged from 51°N–53°N and 44.375°W–45.625°W corresponding to the region shown in Figure 1a with the black box. The forcing includes the zonal and meridional wind stress, shortwave radiation (Q_s), longwave radiation (Q_{long}), and sensible (Q_{sens}) and latent (Q_{lat}) heat fluxes. Figure 2 shows the hourly fluxes obtained from MERRA-2 for the time ranging from yeardays 0 to 100 for 2008 and includes the shortwave (Figure 2a), the net heat flux (Figure 2b), which is the summation of the shortwave and longwave radiative, sensible, and the latent heat fluxes (i.e., $Q_{\text{net}} = Q_s + Q_{\text{long}} + Q_{\text{sens}} + Q_{\text{lat}}$). The zonal wind stress (τ_x) and meridional wind stress (τ_y) are shown in Figures 2c and 2d. In Figure 2, the weekly averaged data are superimposed on the hourly data.

A linear gradient in Q_{net} is imposed in our simulations such that there is a 50 W/m^2 difference between the southern and northern boundaries. This gradient imposes a very simple spatial change in the heat flux in the

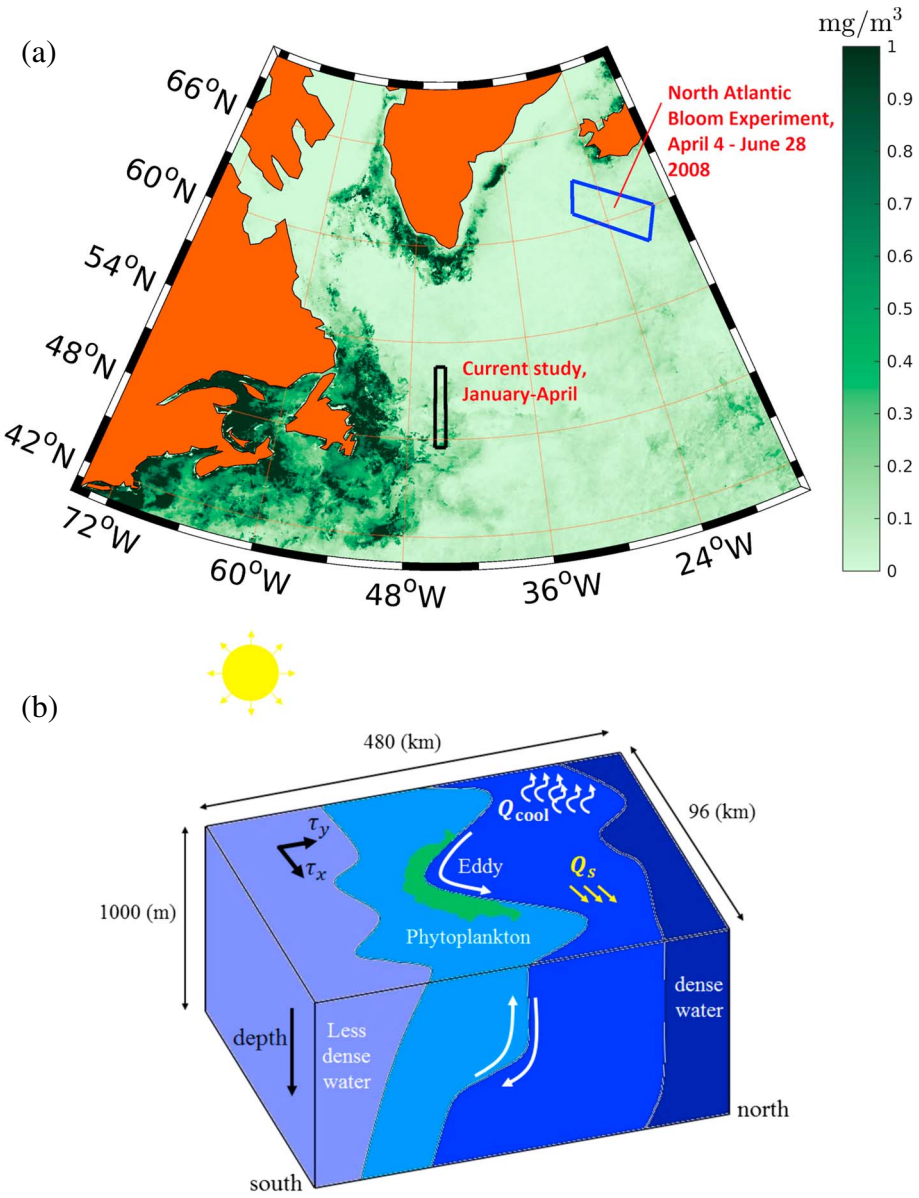

Figure 1. (a) Approximate location of the modeled region in the North Atlantic is shown by the black, solid line box. The concentration of chlorophyll *a* obtained from MODIS-Aqua averaged from yeardays 50–150 is shown in green color. Location of North Atlantic Bloom Experiment carried out in April–June 2008 (Fennel et al., 2011) (solid, blue box) is shown for comparison. (b) A schematic of the modeled domain in the North Atlantic. MODIS = Moderate Resolution Imaging Spectroradiometer.

south-north direction. The average and standard deviation of hourly Q_s, the hourly and weekly averaged Q_{net}, τ_x, and τ_y are presented in Tables 1 and 2, which show a high standard deviation for hourly fluxes.

2.4. Initial Density and Fronts

The model is initialized with a density profile at the northern boundary, identical to that used in the simulations by Mahadevan et al. (2012; Figure 3a, blue line). This initial density profile is also used for the case without fronts. The initial density profile is the averaged profile obtained from NAB08 Seagliders from yeardays 95 to 105 in 2008, deployed at the location shown in Figure 1a. Here for the sake of simplicity, the density is represented by a density anomaly $\sigma_t = \rho - \rho_0$, where ρ is the potential density and $\rho_0 = 1{,}000$ kg/m^3. Figure 3a (blue line) also shows the initial buoyancy frequency which is a measure of the density stratification and is calculated as

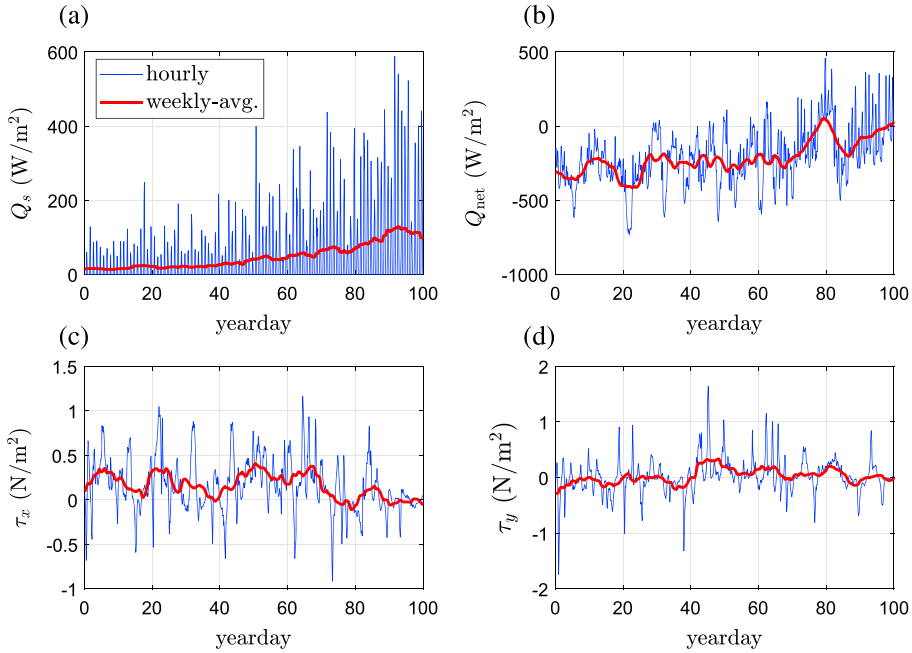

Figure 2. The hourly and weekly averaged fluxes for (a) shortwave radiation (Q_s), (b) net heat flux (Q_{net}), (c) zonal wind stress (τ_x), and (d) meridional wind stress (τ_y), for the region shown in Figure 1.

$$N^2 = \frac{\partial b}{\partial z} = \frac{-g}{\rho_0}\left(\frac{\partial \sigma_t}{\partial z}\right), \tag{5}$$

where $b = (-g/\rho_0)(\rho - \rho_0)$ is the buoyancy. This density profile was used to initialize simulations without fronts. A horizontal density gradient was imposed upon this density profile to generate the initial fronts in the frontal simulations (Figure 3b). Three fronts span the domain in the meridional direction such that the density increases toward the north. The maximum horizontal buoyancy gradient $M_y^2 = (-g/\rho_0)(\partial\sigma_t/\partial y) \approx 3.6\times10^{-8}\ \text{s}^{-2}$, which is close to the density gradient observed in NAB08 conducted in 2008 (Fennel et al., 2011; Mahadevan et al., 2012).

2.5. Biological Model

The phytoplankton evolution model of Bagniewski et al. (2011) described by

$$\frac{\partial P}{\partial t} + \nabla.(\mathbf{u}P) = \mu_P P - m_P P + \frac{\partial}{\partial z}\left(w_s P\right) + \frac{\partial}{\partial z}\left(K_z^d \frac{\partial P}{\partial z}\right), \tag{6}$$

is coupled to PSOM. In this equation, P is the phytoplankton concentration and $\mathbf{u} = (u, v, w)$ is the velocity vector. The parameter μ_P is the growth rate, $m_P = 0.0187\ \text{day}^{-1}$ is the mortality rate, and $w_s = 1.2$ m/day is the sinking rate of phytoplankton. The mortality rate is lower than the value recommended by Bagniewski et al. (2011), because the original model is tuned and tested for spring and leads to very low concentration of phytoplankton in winter.

Table 1
Mean and Standard Deviation of the Hourly Shortwave Radiation (Q_s^{hourly}), Net Hourly Heat Flux (Q_{net}^{hourly}) and Net Weekly Averaged Heat Flux (Q_{net}^{weekly}) for the First 100 Days of 2008 at the Study Region

Flux	Average (W/m^2)	Std (W/m^2)
Q_s^{hourly}	47.97	90.98
$Q_{\text{net}}^{\text{hourly}}$	−212.31	189.98
$Q_{\text{net}}^{\text{weekly}}$	−213.40	108.82

Table 2
Mean and Standard Deviation of the Hourly Zonal Wind Stress (τ_x^{hourly}), the Hourly Meridional Wind Stress (τ_y^{hourly}), the Weekly Averaged Zonal Wind Stress (τ_x^{weekly}) and the Weekly Averaged Meridional Wind Stress (τ_y^{weekly}) at the Study Region for the First 100 Days of 2008

Flux	Average (N/m^2)	Std (N/m^2)
τ_x^{hourly}	0.158	0.297
τ_x^{weekly}	0.159	0.133
τ_y^{hourly}	0.025	0.305
τ_y^{weekly}	0.024	0.127

The phytoplankton growth rate is calculated as

$$\mu_P = \mu_P^{\max} \frac{I_P \alpha_P}{\sqrt{\left(\mu_P^{\max}\right)^2 + \left(I_P \alpha_P\right)^2}}, \tag{7}$$

where $\mu_P^{\max} = 0.536\ \text{day}^{-1}$, and I_P is the photosynthetically active radiation (PAR), which is calculated as

$$I_P = I_0 \phi e^{-zK_w - \int_0^z K_{\text{Chl}} \text{Chl}(\eta) \text{d}\eta}. \tag{8}$$

Here $\alpha_P = 0.0538\ \text{m}^2 \cdot \text{day}^{-1} \cdot \text{W}^{-1}$ is the initial slope of the photosynthesis-irradiance curve. I_0 is the total incoming solar radiation at the surface and $I_0\phi$ is the photosynthetically active radiation with $\phi = 0.43$ (Bagniewski et al., 2011). The chlorophyll (Chl) which is a surrogate for phytoplankton biomass is estimated from the phytoplankton concentration. $K_w = 0.059\ \text{m}^{-1}$ is the coefficient for the attenuation of light in water and $K_{\text{Chl}} = 0.041\ \text{m}^2/\text{mg}$ is the coefficient for light attenuation due to chlorophyll (Bagniewski et al., 2011).

We have neglected nutrient limitation and grazing of phytoplankton by zooplankton for the wintertime simulations. A simulation that spans several seasons would require that equation (6) be coupled to another set of equations governing nutrients and zooplankton. Since our simulations are limited to winter when nutrients are abundant (Sverdrup, 1953) and the grazing pressure from zooplankton is considered insignificant due to deepening of mixed layers (Behrenfeld, 2010), these equations are not incorporated.

In our simulations, phytoplankton within the mixed layer are exposed to the light averaged over the MLD, which is determined as the depth where the density exceeds the density at the surface by 0.01 kg/m^3. This assumption holds if in the mixing layer the turbulent mixing occurs on time scales much shorter than the time scale for the growth of phytoplankton (Mahadevan et al., 2012). We test the suitability of this assumption by comparing the mixing layer depth with the MLD. The turbulent diffusivity (K_z^d) in the meridional direction in the middle of the zonal direction ($x = 48$ km) is shown in Figure 4 for two different days: (a) yearday 60 when there is a strong cooling event, strong mixing occurs and the mixed layer is deep; and (b) yearday 80 when the ocean surface is warming, the mixing is weak and hence the mixed layer is shallow. The MLD (yellow line) is plotted in both figures. In Figure 4, the mixing layer depth is defined as the depth where K_z^d becomes less than 10^{-3} m^2/s and is shown by the magenta line. There is good agreement between the depth of the mixing layer and the MLD. Next, we calculate the relevant phytoplankton growth time scale, $T_{\text{Phy}} = 1/(\mu_P - m_P)$. For yearday 60, with daily averaged incoming solar irradiance ~27 W/m^2, average K_z^d of ~0.56 m^2/s (from Figure 4) and average MLD of ~393 m, the modeled phytoplankton growth time scale changes exponentially from ~2.1 days near surface to ~22 days at $z = -50$ m. In comparison, the relevant time scale for mixing phytoplankton in the actively mixed surface boundary layer is $T_{\text{mix}} = H^2/K_z^d \approx 3.2$ days. Hence, phytoplankton that reside in the MLD mix on time scales shorter than the time scales required for their growth. We can therefore assume that phytoplankton are exposed to the average light in the mixed layer.

3. Results and Discussion

3.1. Hourly Versus Weekly Averaged Forcing

The change in average MLD with time and the depth-integrated phytoplankton down to $z \approx -400$ m are shown in Figure 5 for hourly and weekly averaged forcing, averaged zonally as well as over $y = 100$–400 km. In the rest of the paper the domain averages are taken over this same region. Also, to better illustrate the

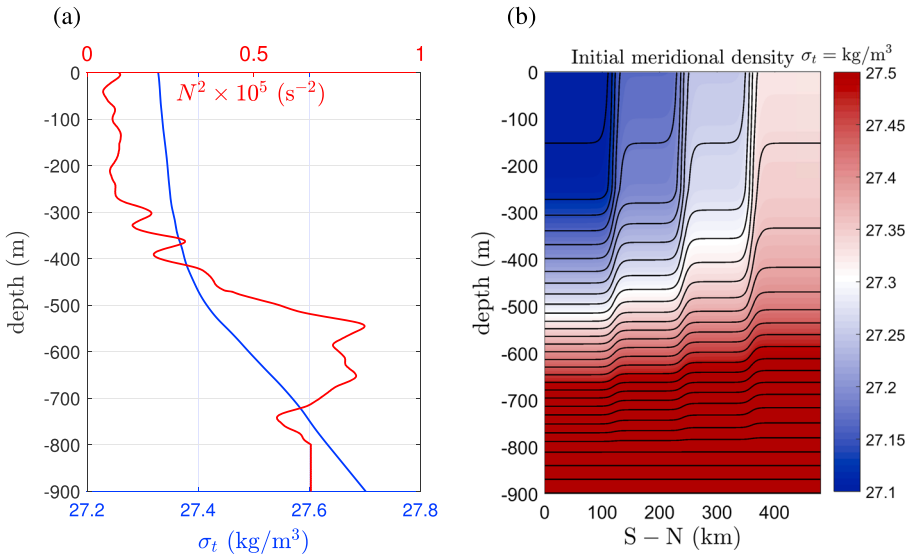

Figure 3. (a) The initial density profile and buoyancy frequency used for the case without fronts and also used as the initial condition at the northern boundary (i.e., y = 480 km) for the frontal case. (b) The initial density distribution in case with fronts in the meridional (y) direction, where solid black lines show the contours of density. Here $\sigma_t = (\rho - 1,000)$ kg/m^3 is the density anomaly.

effect of forcing on the MLD evolution and its influence on the phytoplankton growth in winter, two additional numerical simulations are implemented without fronts and with the same hourly and averaged fluxes.

Due to intermittency of the hourly Q_{net} and wind stress, the mixed layer stratification changes within days (Figure 5a), particularly in the case with fronts. However, comparison of the average phytoplankton concentration from hourly and weekly averaged fluxes in Figure 5b does not show a significant difference. This surprising result is in contrast to the expectation that when MLD shoals in winter, the phytoplankton production should increase accordingly. The major difference between the hourly and weekly averaged cases is the timing of the bloom and phytoplankton growth after the bloom. The bloom occurs earlier in the weekly averaged case and with a higher growth rate.

To assess the reason for the relative insensitivity of phytoplankton to the high episodic fluxes, we examine the time scales pertinent to phytoplankton growth. The smallest growth time scale for our model is

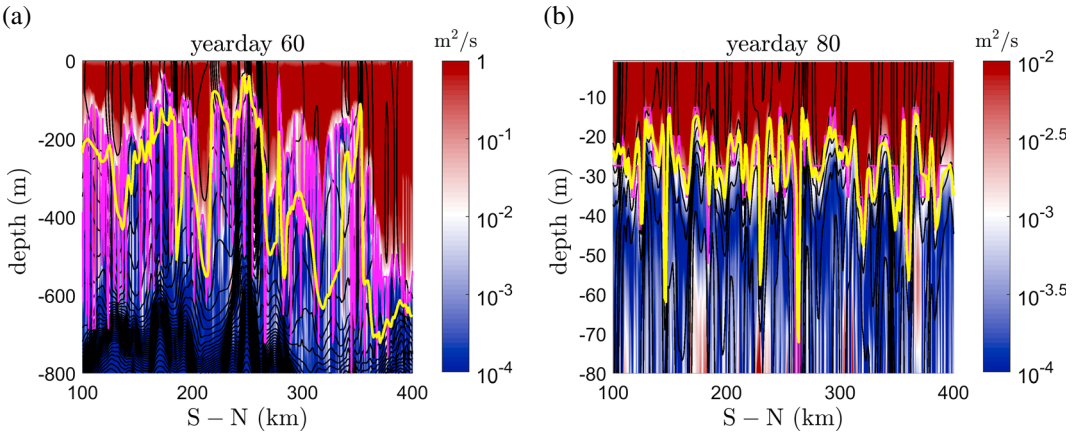

Figure 4. The turbulent diffusivity (K_z^d) and the mixed layer in the meridional direction at (a) yearday 60 and (b) yearday 80. The yellow line shows the MLD and the magenta line is the computed mixing layer depth. Yearday 60 is a time of strong cooling with deep MLD, and yearday 80 incurs a warming event with shallow MLD. In both cases, the region of active mixing agrees reasonably well with the MLD although it is shallower than the MLD in some regions for strong cooling at yearday 60. MLD = mixed layer depth.

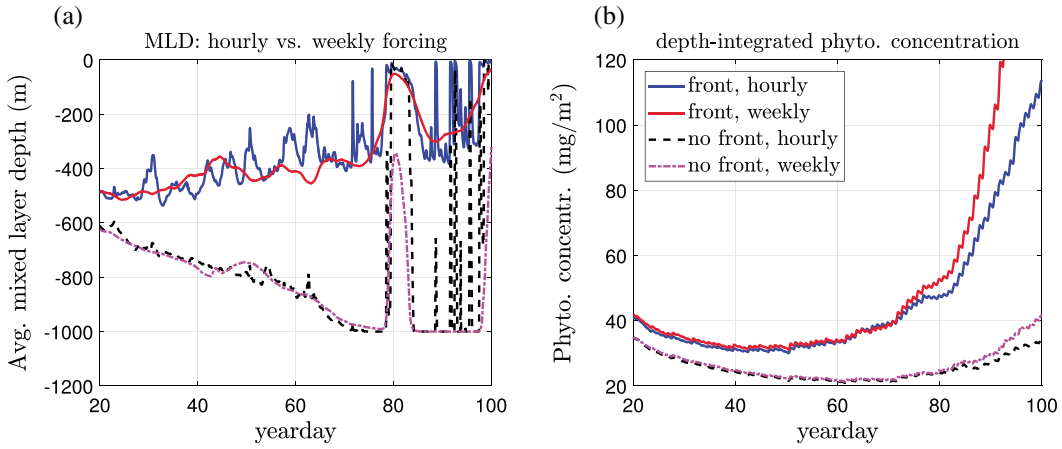

Figure 5. Comparison of hourly forcing and weekly averaged forcing on (a) the average MLD and (b) the depth-integrated phytoplankton concentration. The cases without fronts show substantially deeper mixed layer depths and lower phytoplankton concentration compared to the cases with fronts. The sudden changes of the MLD for the no front case (e.g., around yearday 80) is due to the sudden change in Q_{net} seen in Figure 2b. MLD = mixed layer depth.

$T_{Phy}^{min} = 1/(\mu_P^{max} - m_P) \approx 1.95$ days. Moreover, the net heat flux (Q_{net}) for yeardays 60–80 (Figure 6) shows that except after yearday ~77, most positive net heat fluxes (Q_{net}) last a fraction of a day. Consequently, ML also shoals only for a fraction of a day as seen in Figure 5a. Therefore, before phytoplankton have sufficient time to grow, the MLD deepens. To test the effect of phytoplankton growth time scale, we performed a new set of idealized simulations for several phytoplankton growth time scales ranging from 0.3 to 14.2 days, with constant wind stresses as $\tau_x = 0.158$N/m^2 and $\tau_y = 0.025$N/m^2, and constant shortwave radiation $Q_s = 47.97$ W/m^2 and variable net heat flux with average value $\overline{Q}_{net} = -212.31$ W/m^2 as shown in Figure 7a. The wind stresses and the average heat fluxes are the averaged fluxes for the first 100 days of 2008 as listed in Tables 1 and 2. For these simulations, there are alternate warming and cooling events every 5 days. Each warming or cooling event lasts for one day and varies sinusoidally during the time of occurrence with an amplitude of 315 W/m^2. The Q_{net} standard deviation is ~65 W/m^2 comparable to the standard deviation of the actual Q_{net} presented in Table 1. For better illustration of the net heat flux (Q_{net}), Figure 7a only shows the first 25 days. Results for three time scales $T_{Phy}^{min} = 0.3, 1.95$ and 14.2 days (Figure 7b) show that as we expect, for the long phytoplankton growth time scale of $T_{Phy}^{min} = 14.2$ days the average phytoplankton concentration for constant forcing and variable forcing are very similar. With decrease in T_{Phy}^{min}, phytoplankton concentration increases for both forcing conditions and the difference in phytoplankton concentration between variable forcing and constant forc-

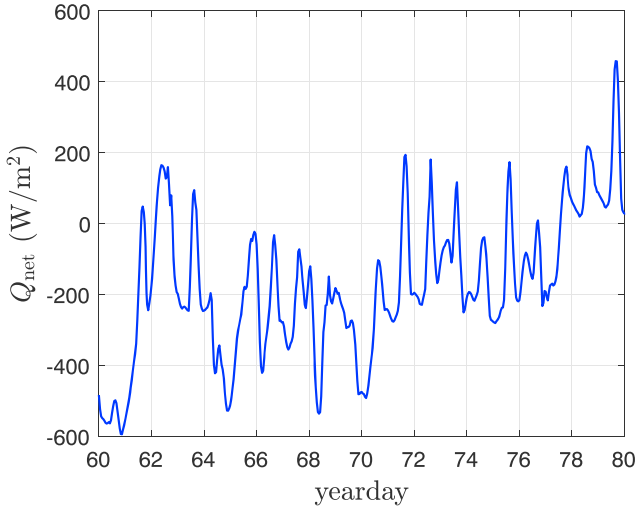

Figure 6. The neat heat flux (Q_{net}) for yeardays 60–80. Most warming events last less than a day and hence are shorter than the growth time scale of phytoplankton.

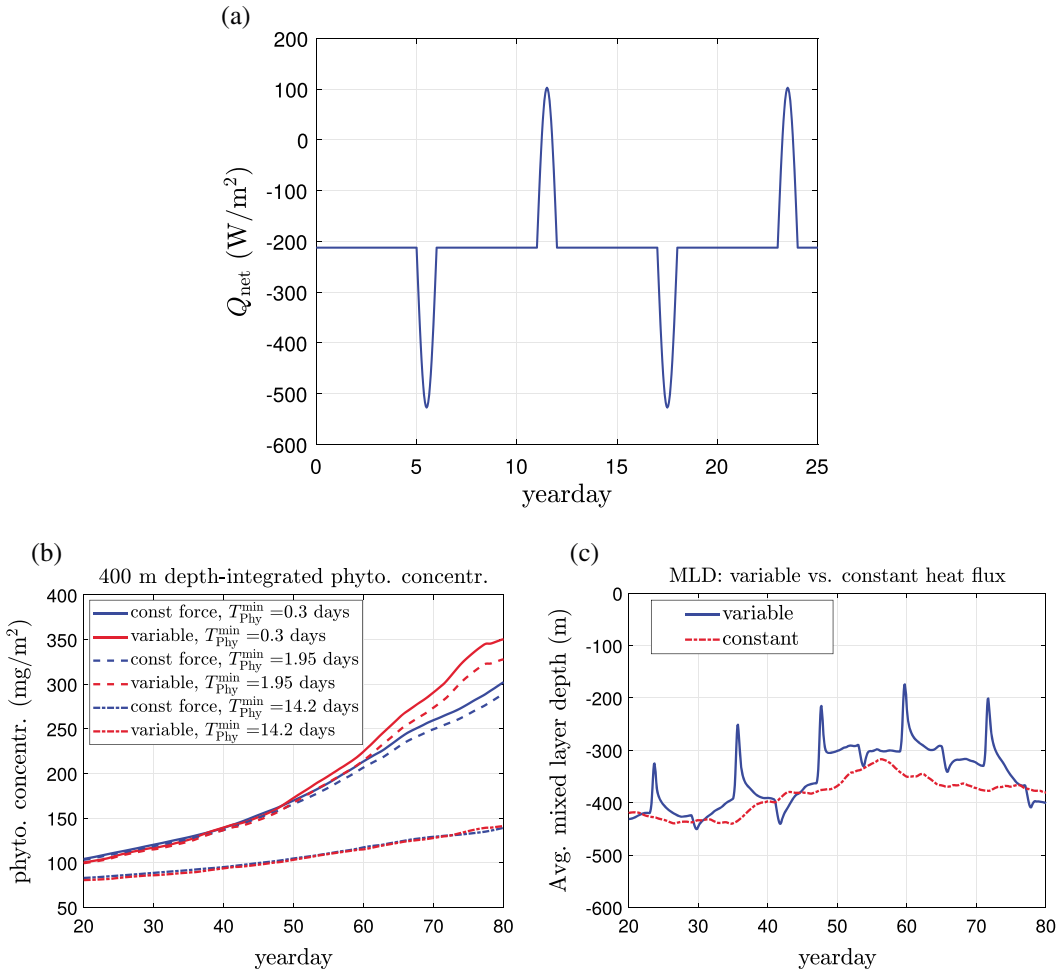

Figure 7. The average phytoplankton concentration for different growth time scales and forcing. MLD = mixed layer depth.

ing grows. However, the difference between the phytoplankton concentration for the constant and variable forcing for each of these time scales is not significant.

To better understand the reason for insensitivity of phytoplankton growth to intermittent air-sea fluxes, we need to take into account the role of MLD. In Figure 7c, the average MLD is about 300–400 m. In spite of the intermittent shoaling due to variable air-sea fluxes, the average MLD transiently shoals to ~200 m. Considering that ML is very deep in winter, phytoplankton that get transported to the euphotic layer have insufficient time to grow. Moreover, the nights in the subpolar regions during winter are long and solar radiation is absent for most of the day, meaning that conditions are not conducive for phytoplankton growth. Hence, during winter when forced with intermittent fluxes, phytoplankton do not have considerably better conditions for growth than when the forcing is averaged weekly.

3.2. Effect of Fronts

Figure 5a shows that due to the slumping of fronts and the consequent restratification, the average MLD in cases with fronts is substantially shallower than the cases without fronts. These differences persist for time scales much longer than $T_{\rm Phy}$. Shallower mixed layers resulting from frontal instabilities increase phytoplankton residence time in the euphotic layer, resulting in their growth (Mahadevan et al., 2012). The results from Figure 5b confirm the fundamental effect of fronts and mixed layer instabilities on production and sustenance of phytoplankton population in wintertimes, where for both hourly and weekly averaged fluxes including fronts results in enhanced production of phytoplankton. The role of fronts has been previously appreciated in studies on the spring bloom showing that the restratification due to fronts is a key parameter for the early initiation of the spring bloom of phytoplankton (Mahadevan et al., 2012). Moreover, in the frontal cases phytoplankton start to slightly increase around yearday 50, which is a few weeks before the time that $Q_{\rm net}$

becomes positive. In the cases without fronts, phytoplankton grow at very weak rates around yearday 70. In the frontal case, the growth accelerates after yearday 70, which corresponds to rapid shoaling of the mixed layer as a result of subsidence in cooling and wind stress (see Figure 2). In a study conducted in the subpolar North Atlantic, by using vertical profiles from floats, Mignot et al. (2018) observed weak growth of phytoplankton in the early winter and rapid growth of phytoplankton in spring when the cooling subsides and mixed layer shoals.

So far we have focused on the variation of the average MLD and phytoplankton. Now, we briefly evaluate how phytoplankton and the MLD change spatially when fronts are present. To that end, we show the MLD as well as the phytoplankton concentration at $z \approx -5.85$m in Figures 8a and 8b. The results we show here are for yearday 60 at midnight and do not change significantly for other times of the day. We can see that there is high spatial variability in the MLD and phytoplankton. Also, the distribution of the MLD agrees fairly well with the distribution pattern of phytoplankton in the domain such that the phytoplankton concentration is normally more where the MLD is shallow and low where the MLD is deep, leading to patches of phytoplankton in the domain. The same agreement between the MLD and the phytoplankton concentration can also be seen in Figures 8c and 8d. Figure 8c shows the phytoplankton concentration and the MLD in the meridional direction at $x = 12$ km, where the yellow line is the MLD, and Figure 8d is a three-dimensional representation of the phytoplankton concentration as well as the MLD (yellow line).

In spite of relatively good agreement between the MLD and the phytoplankton concentration, it is clear that especially near the south, the mixed layer is deep while the phytoplankton concentration is high. In our three-dimensional simulations, phytoplankton get advected between different regions of the flow. A mechanism that contributes to advection is the Ekman transport that, due to the dominant down-front, eastward wind in our simulations, transports phytoplankton toward the south. Also, as the phytoplankton mortality time scale is long, advected phytoplankton do not decrease quickly in the south. A Lagrangian study could reveal better how phytoplankton evolve in different phases of the day and in different places in the domain, which is beyond the scope of the current study. In the next section, we will discuss the effect of numerical resolution on the variability of the MLD and the phytoplankton concentration and highlight the importance of resolving submesoscale fronts.

3.3. Effect of Frontal Strength and Spatial Resolution

The results discussed so far highlight the undeniable effect of fronts on the production and sustenance of the phytoplankton population in winter, meaning that resolving fronts and their related instabilities in numerical models will help better predict the fate of phytoplankton. The criterion for determining the grid resolution is the Rossby radius of deformation (L_R), which is defined as

$$L_R = \frac{NH}{f}, \tag{9}$$

where f is the Coriolis frequency and H is the relevant water depth (i.e., the MLD). The Rossby radius of deformation, which essentially shows the competition of buoyancy and rotational forces (i.e., larger Rossby radius means that buoyancy forces are more dominant) is the threshold above which the flow starts to become geostrophic. In order to resolve submesoscale eddies, which occur at scales where effects of geostrophic balance diminish, the spatial resolution has to be sufficiently smaller than L_R. Considering initial conditions shown in Figure 3b, we can estimate the L_R for our studied case as

$$L_R = \frac{NH}{f} \sim \frac{\left(\sim 1 \times 10^{-3}(\mathrm{s}^{-1})\right) \times \sim 300(\mathrm{m})}{1.114 \times 10^{-4}(\mathrm{s}^{-1})} \sim 2,700\ \mathrm{m}, \tag{10}$$

where $f = 1.114 \times 10^{-4}$ s^{-1} is the Coriolis (inertial) frequency at 50°N. Therefore, the spatial resolution for capturing submesoscale processes needs to be at least $\Delta x, \Delta y \sim 1/4 \times 2{,}700$ m to resolve an instability wave length. The simulations discussed thus far, for which the spatial resolution was 1 km, can marginally resolve submesoscale processes. We next address the impact of spatial resolution.

Most models lack the required grid resolution to resolve submesoscale eddies and frontal processes. To investigate the effect of resolution, we consider four cases with $\Delta x = \Delta y = 0.75, 1, 2$, and 4 km, where only the 0.75, 1, 2 km cases have resolutions smaller than L_R. The results are shown in Figure 9. Also, the case without fronts previously presented in Figure 5 is added for comparison. Clearly, there is direct relation between the

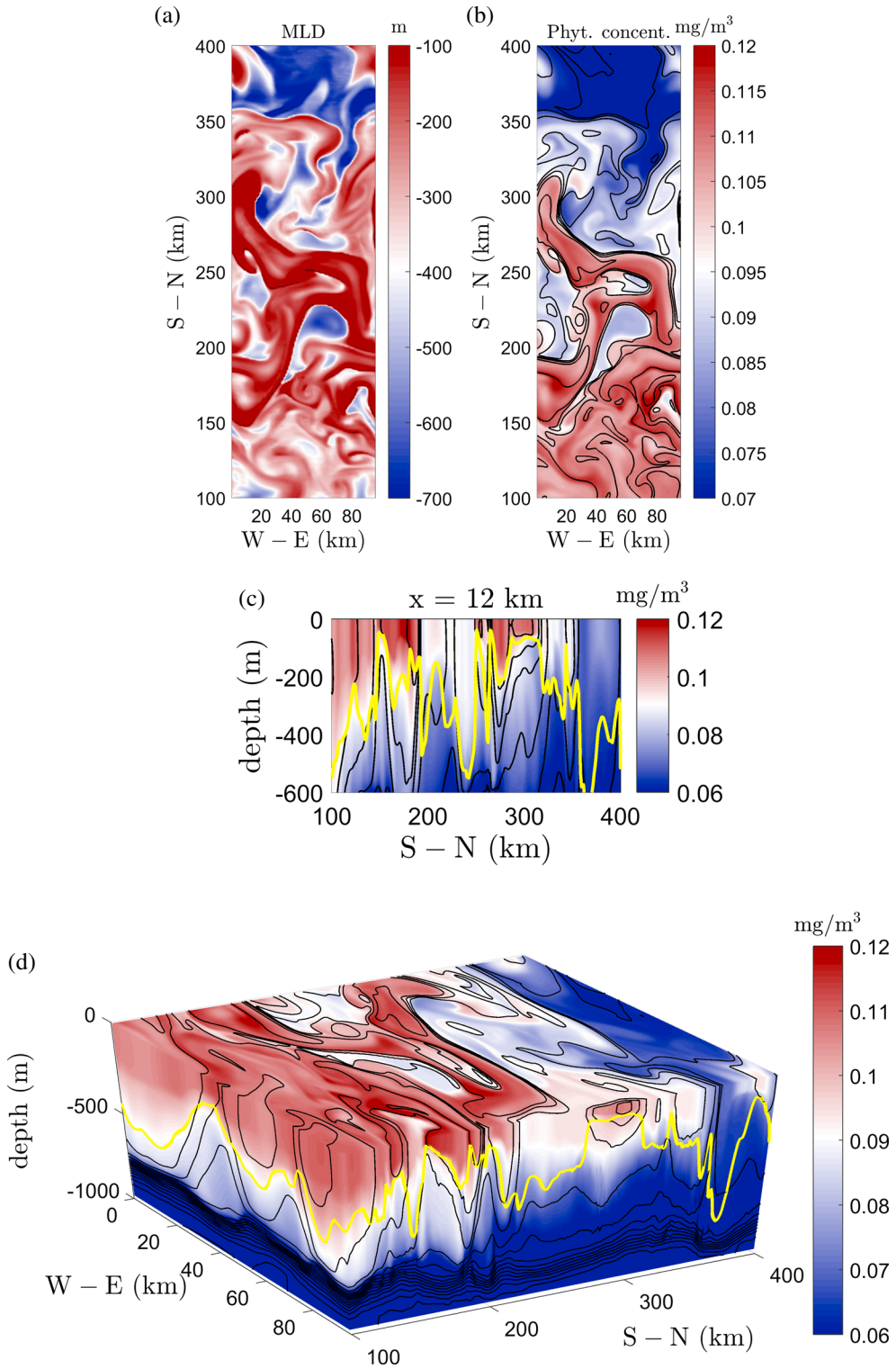

Figure 8. The simulation results at yearday 60 at midnight showing (a) the mixed layer depth, (b) the concentration of phytoplankton on the horizontal surface at $z \approx -5.85$ m, (c) the phytoplankton concentration in the meridional direction at $x = 12$ km, and (d) the phytoplankton concentration at $x = 96$ km, $y = 100$ km and the surface. The yellow solid line in Figures 8c and 8d shows the mixed layer depth.

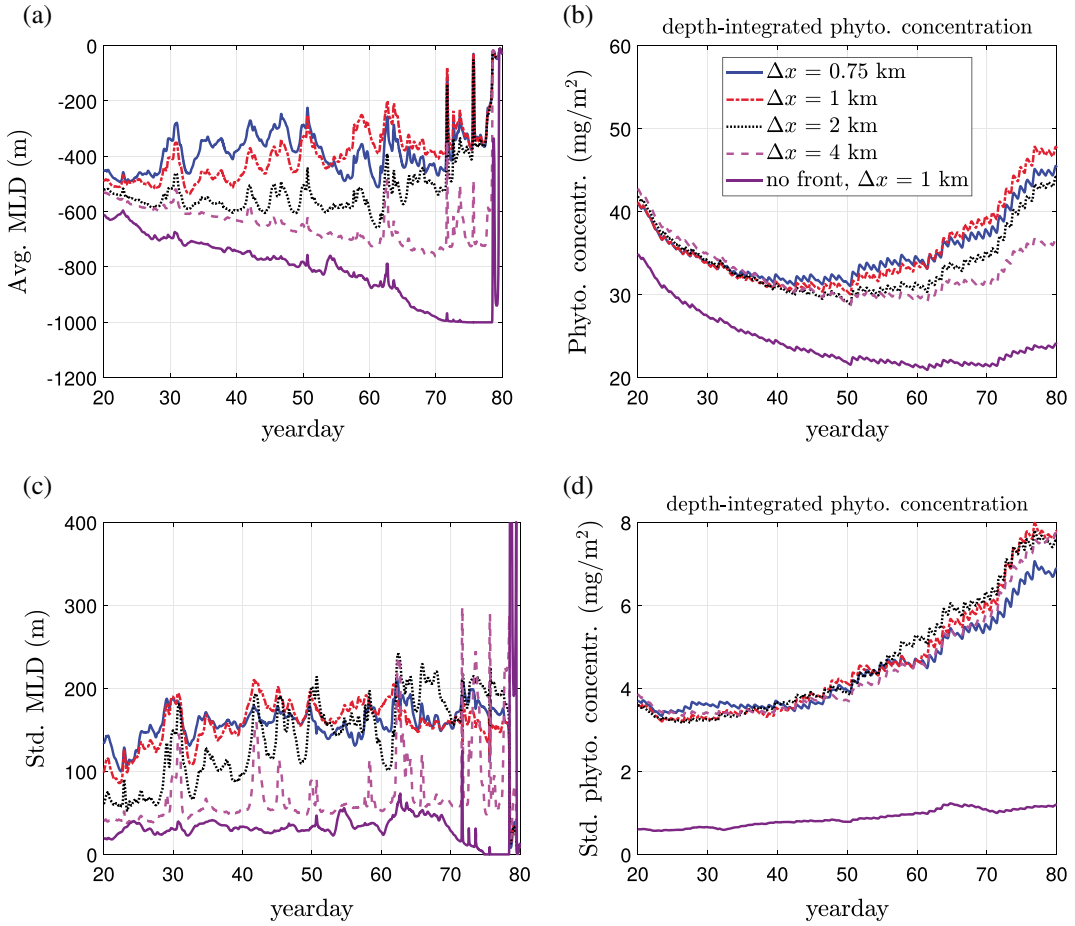

Figure 9. (a) Comparison of the average MLD, (b) the depth-integrated phytoplankton concentration, (c) the standard deviation of the MLD, and (d) the standard deviation of the depth-integrated phytoplankton concentration, for the grid resolutions of 0.75, 1, 2, and 4 km and without fronts case with 1 km resolution.

shoaling of the ML and the spatial resolution (Figure 9a). The ML is shallower for numerical simulations with $\Delta x = 0.75$ and 1 km and relatively shallow for 2 km resolution, which can better resolve submesoscale processes. For the coarse case, the mixed layer is deep but still shallower than the case without fronts. The effect of numerical resolution and frontal strength on mixed layers is also reflected in the production of phytoplankton in winter. In the 0.75 and 1 km resolution simulations, the production of phytoplankton is large due to the shallower mixed layer, which provides the opportunity for phytoplankton to be exposed to sunlight for longer time scales and hence grow more.

The standard deviation of the MLD (Figure 9c) shows that the variability of the MLD is higher for increased model resolutions. There is a noticeable difference between 0.75, 1, and 2 km with 4 km resolutions. The case without fronts has a much smaller standard deviation compared to cases with fronts, highlighting the effect of fronts on the patchiness of the MLD. As for the phytoplankton concentration, all the cases with fronts have similar standard deviation, showing no clear relation between the numerical resolution and the variability in phytoplankton (Figure 9d). However, similar to the MLD, without fronts the standard deviation of the phytoplankton concentration is much less than the cases with fronts, signifying the role of fronts on the patchiness of phytoplankton. We consider the variability of the MLD and phytoplankton for different numerical resolutions by plotting their histograms in Figure 10. While the increase of the numerical resolution leads to higher variability in the MLD, the phytoplankton variability is unchanged. As previously shown in Figure 9d, phytoplankton variances are similar for different resolutions; however, phytoplankton concentrations from higher-resolution models are shifted toward higher values. The dashed lines on Figure 10 illustrate the average MLD and the phytoplankton concentration. With increasing spatial resolution, the MLD shallows and the primary productivity increases.

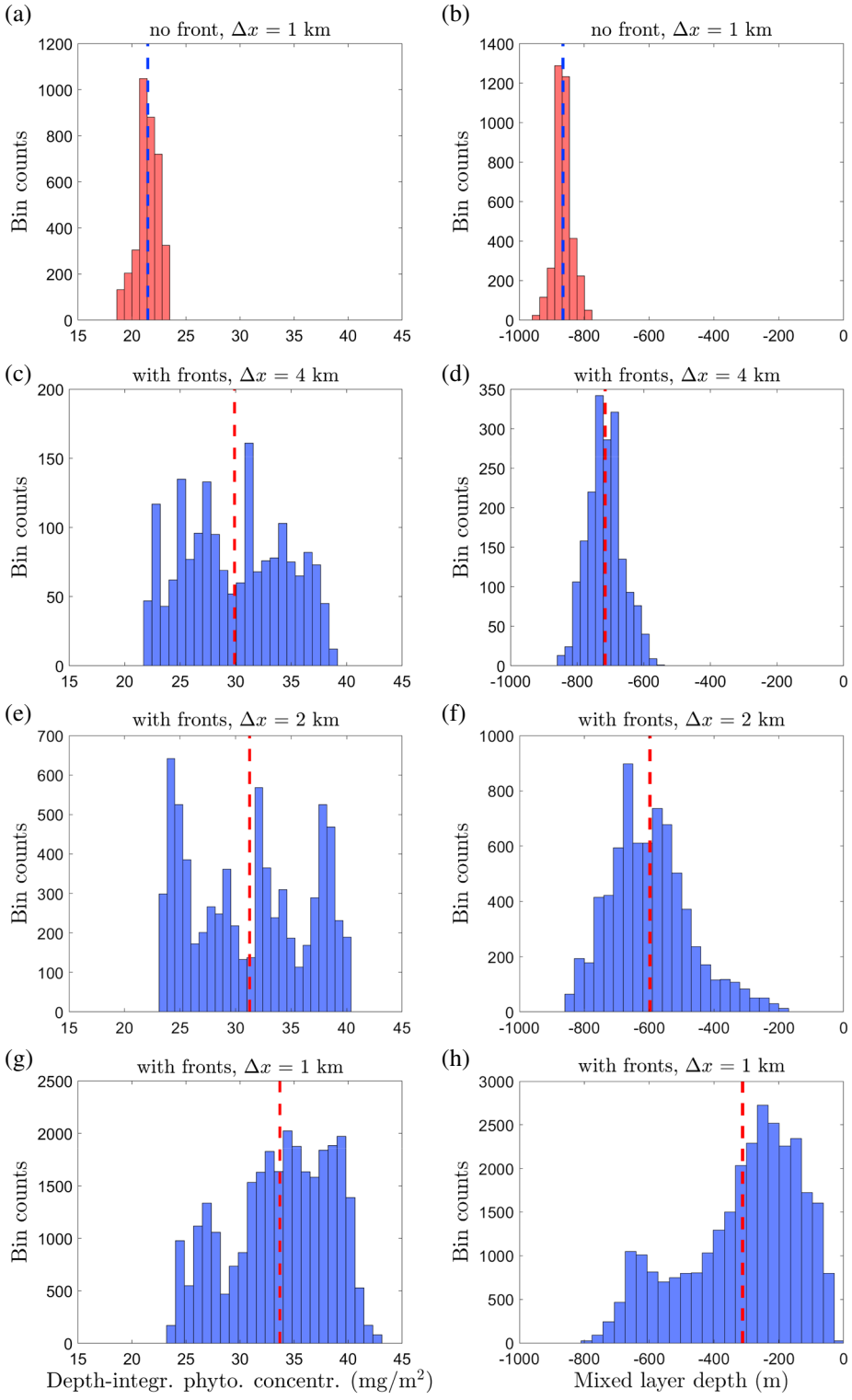

Figure 10. The histograms of the phytoplankton concentration integrated down to $z \approx -400$ m and the mixed layer depth, for yearday 60 obtained from the numerical simulation for (a, b) a case without fronts; and different numerical resolutions (c, d) 4 km, (e, f) 2 km, and (g, h) 1 km. The dashed, vertical line shows the average value.

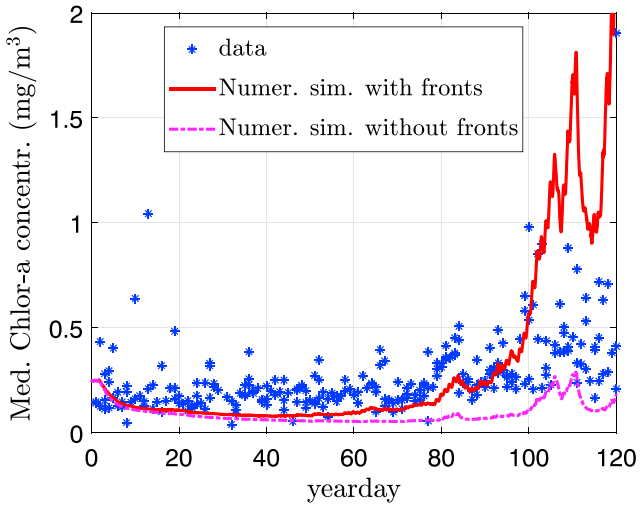

Figure 11. Comparison of the median chlorophyll *a* concentration between the longitude 20°W–45°W and the latitude 47°N–53°N obtained from MODIS-Aqua with the median of the phytoplankton concentration at $z \approx -5.85$m, obtained from the numerical simulation with $\Delta x = \Delta y = 1$ km. Results for the case without fronts are also shown for comparison. Clearly, when fronts are present the simulation results show better agreement with data both in winter and early spring. MODIS = Moderate Resolution Imaging Spectroradiometer.

3.4. Comparison With Satellite Data

As mentioned in section 2.2, the numerical domain is idealized and does not include all the complex processes in the study region. A comparison of the numerical simulation results with chlorophyll *a* (Chl*a*) in the ocean could reveal how this and other model idealizations influence the results. Chlorophyll *a* (Chl*a*) data for year 2008 have been obtained from Moderate Resolution Imaging Spectroradiometer (MODIS) aboard National Aeronautics and Space Administration's Aqua satellite that was launched in May 2002. MODIS-Aqua has two spectroradiometers that operate in two bands from 620 nm to 670 nm and from 841 to 876 nm, each with an along-track and cross-track resolution of 250 m. These ranges have the sufficient sensitivity for detecting the color changes in the ocean water (Chen et al., 2007).

Figure 11 compares the time series of the Chl*a* median in 2008 from MODIS-Aqua and the median of the phytoplankton concentration from the numerical simulation. MODIS-Aqua data are obtained over an area limited between longitude 20°W–45°W and latitude 47°N–53°N. The median of the phytoplankton concentration from the numerical simulation is calculated at $z \approx -5.85$ m, from $x = 0$–96 km and $y = 100$–400 km. Also, the phytoplankton concentration from simulations without fronts is included for comparison. Satellite and simulation results show that persistent growth starts from yearday ~80. Although the numerical simulation results show good agreement with the data, after spring initiation the phytoplankton concentration from simulation is higher than the concentration derived from satellite data. Besides neglecting many complex processes of this region in the model, this difference could be attributed to the absence of grazing of phytoplankton by zooplankton and abundance of nutrients in our model as described in equation (6). Also, we use a constant mortality rate for winter simulations which needs to be modified with the start of spring.

In Figure 12, we compare the histogram of the Chl*a* from MODIS-Aqua between the longitude 20°W–45°W and the latitude 47°N–53°N with the histogram of phytoplankton from the simulation results at $z \approx -5.85$ m, from $x = 0$–96 km and $y = 100$–400 km. The histogram of the satellite chlorophyll *a* concentration in Figure 12a shows a log-normal distribution that is consistent with Campbell (1995). The simulation results in Figure 12b look significantly different from data with much smaller variability. In our simulations, we solve a simplified model for only one phytoplankton species in a relatively small domain and do not incorporate competition between different types of phytoplankton. Also, as shown in Figures 9 and 10 the phytoplankton concentration is dependent on numerical resolution. There are many scales between the grid size and the phytoplankton scale that our model cannot resolve. Hence, the grid resolutions we use for the size of our domain cannot capture all the instabilities and turbulent processes that cause the variability in the phytoplankton population. Again, here we have assumed that zooplankton grazing is negligible, nutrients are abundant and are uniformly distributed in the mixed layer. These limitations and simplifications can potentially influence

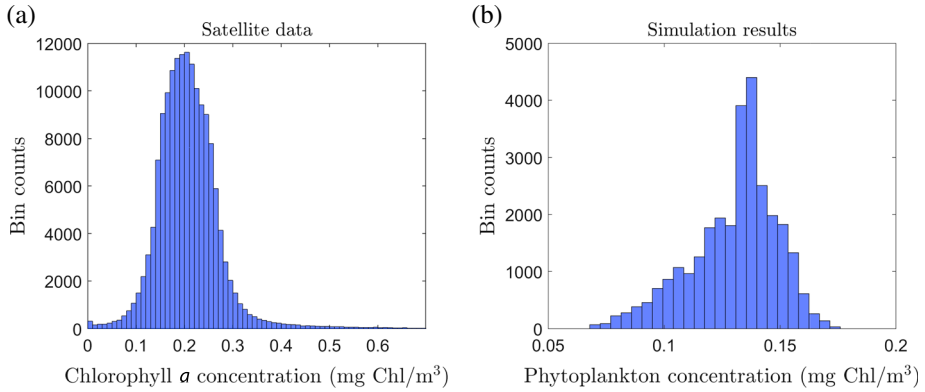

Figure 12. The histogram of (a) the chlorophyll *a* concentration averaged on the longitude 20°W–45°W and the latitude 47°N–53°N obtained from MODIS-Aqua in 2008, and (b) the surface-averaged phytoplankton concentration at $z \approx -5.85$ m obtained from the numerical simulation. MODIS = Moderate Resolution Imaging Spectroradiometer.

the distribution of phytoplankton and result in a different variability in the phytoplankton concentration in numerical simulations.

4. Concluding Remarks

Results from idealized simulations in a process model show that while strong winds and loss of heat in the subpolar North Atlantic during winter lead to deep mixed layers and keep the mixed layer unstratified, the restratifying effect of fronts is still at play and results in shallower mixed layers than would exist without fronts. The simulations predict that without fronts the mixed layer deepens constantly during winter, while with fronts, the average MLD is about 400 m and about 600 m shallower than the average MLD without fronts. Fronts also create spatially variable stratification with shallow mixed layers across the domain. Our simulations predict that increase in frontal strength leads to decrease of the average MLD and increase in the patchiness of the MLD.

Phytoplankton growth substantially increases in winter simulations that include fronts. While in many parts of the modeled ocean, phytoplankton dwindle due to deep mixed layers, fronts generate regions of enhanced stratification or shallower mixed layer, where phytoplankton can survive and grow as they have the opportunity to be exposed to sunlight for longer periods. Moreover, the shallower mixed layer prevents the dilution of phytoplankton and their export to the deep ocean, which is also fundamental for sustaining phytoplankton during winter. The high concentration and production of phytoplankton near fronts contribute to the sustenance and productivity of phytoplankton during winter in the subpolar North Atlantic, where light is scant. This sustenance of phytoplankton is essential for providing the seed population for the spring bloom, where the increase of sunlight and heat and hence restratification allow the exponential growth of phytoplankton. Additionally, stronger fronts, which have shallow average MLD, cause higher production of phytoplankton compared to weak fronts.

Besides fronts, high variability of air-sea fluxes can cause restratification of the mixed layer and change in the MLD. Simulations suggest that the transient shoaling (or deepening) caused by variable air-sea fluxes has little effect on the production of phytoplankton mainly due to relatively deep mixed layers in winter and short time scales of episodic air-sea fluxes compared to phytoplankton growth time scales, which are on the order of days. Other important reasons for the insensitivity of phytoplankton growth to the variability in air-sea fluxes are short days and weak light intensity implying slow growth during winter in the subpolar North Atlantic.

The assumptions used in this idealized study include only one phytoplankton species, light-dependent growth, and constant mortality rates. Further, zooplankton and nutrients are not explicitly modeled. While resolving mixed layer instabilities, our numerical simulations do not account for all subgrid-scale processes that influence mixing and transport in the ocean. It would be interesting in a future study to consider the competition between different phytoplankton species and also use a Lagrangian approach to evaluate how fronts and resultant patchiness can increase the residence time of phytoplankton in regions of shallow mixed layer and contribute to their growth during winter in the subpolar North Atlantic.

Acknowledgments
The simulation data can be downloaded from https://zenodo.org/record/1229458#.WuD6t9Yh1hF. The MERRA-2 data can be obtained from https://gmao.gsfc.nasa.gov/reanalysis/MERRA-2/. The MODIS-Aqua data can be downloaded from https://oceancolor.gsfc.nasa.gov/data/aqua/. The PSOM code can be downloaded from https://github.com/PSOM/. F. K. and A. T. acknowledge the support from the National Science Foundation under grant OCE-1434512. A. M. acknowledges funding from the National Science Foundation under grant OCE-1434788.

References

Backhaus, J. O., Hegseth, E. N., Wehde, H., Irigoien, X., Hatten, K., & Logemann, K. (2003). Convection and primary production in winter. *Marine Ecology Progress Series*, *251*, 1–14.

Bagniewski, W., Fennel, K., Perry, M. J., & D'Asaro, E. A. (2011). Optimizing models of the North Atlantic spring bloom using physical, chemical and bio-optical observations from a Lagrangian float. *Biogeosciences*, *8*, 1291–1307.

Behrenfeld, M. J. (2010). Abandoning Sverdrup's critical depth hypothesis on phytoplankton blooms. *Ecology*, *91*, 977–989.

Boccaletti, G., Ferrari, R., & Fox-Kemper, B. (2007). Mixed layer instabilities and restratification. *Journal of Physical Oceanography*, *837*, 2228–2250.

Bosilovich, M. G., Akella, S., Coy, L., Cullather, R., Draper, C., Gelaro, R., et al. (2015). Technical report series on global modeling and data assimilation. NASA.

Boss, E., & Behrenfeld, M. (2010). In situ evaluation of the initiation of the North Atlantic phytoplankton bloom. *Geophysical Research Letters*, *37*, L18603. https://doi.org/10.1029/2010GL044174

Brody, S. R., & Lozier, M. S. (2010). Changes in dominant mixing length scales as a driver of subpolar phytoplankton bloom initiation in the North Atlantic. *Geophysical Research Letters*, *41*, 3197–3203. https://doi.org/10.1002/2014GL059707

Burchard, H., Bolding, K., & Villareal, M. R. (1999). GOTM, a general ocean turbulence model: Theory, implementation and test cases (*Tech. Rep. EUR 18745 EN*). Europe: European Commission.

Callies, J., Ferrari, R., Klymak, J. M., & Gula, J. (2015). Seasonality in submesoscale turbulence. *Nature Communications*, *6*, 6862.

Campbell, J. W. (1995). The lognormal distribution as a model for bio-optical variability in the sea. *Journal of Geophysical Research*, *100*, 13,237–13,254.

Chen, Z., Chuanmin, H., & Muller-Karger, F. (2007). Monitoring turbidity in Tampa Bay using MODIS/Aqua 250-m imagery. *Remote Sensing of Environment*, *109*, 207–220.

D'Asaro, E. A. (2008). Convection and the seeding of the North Atlantic bloom. *Journal of Marine Systems*, *69*, 233–237.

Fennel, K., Cetinić, I., D'Asaro, E., Lee, C., & Perry, M. J. (2011). Autonomous data describe North Atlantic spring bloom. *Earth and Space Science News: Eos*, *92*, 465–466.

Fox-Kemper, B., Ferrari, R., & Hallberg, R. (2008). Parameterization of mixed layer eddies. Part I: Theory and diagnosis. *Journal of Physical Oceanography*, *38*, 1145–1165.

Huisman, J., Arrayás, M., Ebert, U., & Sommeijer, B. (2002). How do sinking phytoplankton species manage to persist? *The American Naturalist*, *159*, 245–254.

Huisman, J., van Oostveen, P., & Weissing, F. J. (1999). Critical depth and critical turbulence: Two different mechanisms for the development of phytoplankton blooms. *Limnology and Oceanography*, *44*, 1781–1787.

Jones, W. P., & Launder, B. E. (1972). The prediction of laminarization with a two-equation model of turbulence. *International Journal of Heat and Mass Transfer*, *15*, 301–314.

Karimpour, F., & Venayagamoorthy, S. K. (2014). A simple turbulence model for stably stratified wall-bounded flows. *Journal of Geophysical Research: Oceans*, *119*, 870–880. https://doi.org/10.1002/2013JC009332

Lacour, L., Ardyna, M., Stec, K. F., Claustre, H., Prieur, L., Poteau, A., et al. (2017). Unexpected winter phytoplankton blooms in the North Atlantic subpolar gyre. *Nature Geoscience*, *10*, 836–839.

Large, W. G., McWilliams, J. C., & Doney, S. C. (1994). Oceanic vertical mixing: A review and a model with a nonlocal boundary layer parameterization. *Reviews of Geophysics*, *32*, 363–403.

Luo, H., Bracco, A., Cardona, Y., & McWilliams, J. C. (2016). Submesoscale circulation in the northern Gulf of Mexico: Surface processes and the impact of the freshwater river input. *Ocean Modelling*, *101*, 68–82.

Mahadevan, A. (2006). Modeling vertical motion at ocean fronts: Are nonhydrostatic effects relevant at submesoscales? *Ocean Modelling*, *14*, 222–240.

Mahadevan, A. (2016). The impact of submesoscale physics on primary productivity of plankton. *Annual Review of Marine Science*, *8*, 161–184.

Mahadevan, A., D'Asaro, E., Lee, C., & Perry, M. J. (2012). Eddy-driven stratification initiates North Atlantic spring phytoplankton blooms. *Science*, *337*, 54–58.

Mahadevan, A., Tandon, A., & Ferrari, R. (2010). Rapid changes in mixed layer stratification driven by submesoscale instabilities and winds. *Journal of Geophysical Research*, *115*, C03017. https://doi.org/10.1029/2008JC005203

McGillicuddy, D. J. Jr. (2016). Mechanisms of physical-biological-biogeochemical interaction at the oceanic mesoscale. *Annual Review of Marine Science*, *8*, 125–159.

Mignot, A., Ferrari, R., & Claustre, H. (2018). Floats with bio-optical sensors reveal what processes trigger the North Atlantic bloom. *Nature Communications*, *9*, 190.

Miller, S. B., & Wheeler, P. A. (2012). *Biological oceanography*. Hoboken, New Jersey, United States: John Wiley Sons.

Plueddemann, A. J., Weller, R. A., Stramska, M., Dickey, T. D., & Marra, J. (1995). Vertical structure of the upper ocean during the marine light–mixed layers experiment. *Journal of Geophysical Research*, *100*, 6605–6619.

Pope, S. B. (2000). *Turbulent flows*. Cambridge: Cambridge Univ. Press.

Riley, G. A., Stommel, H., & Bumpus, D. F. (1949). Quantitative ecology of the plankton of the western North Atlantic. *Bulletin of the Bingham Oceanographic Collection Yale University*, *12*, 1–169.

Rossby, T. (1996). The North Atlantic current and surrounding waters: At the crossroads. *Reviews of Geophysics*, *34*, 463–481.

Sabine, C. L., Feely, R. A., Gruber, N., Key, R. M., Lee, K., Bullister, J. L., et al. (2004). The oceanic sink for anthropogenic CO_2. *Science*, *305*, 367–371.

Sverdrup, H. U. (1953). On conditions for the vernal blooming of phytoplankton. *Journal du Conseil/Conseil Permanent International pour l'Exploration de la Mer*, *18*, 287–295.

Takahashi, T., Sutherland, S. C., Wanninkhof, R., Sweeney, C., Feely, R. A., Chipman, D. W., et al. (2009). Climatological mean and decadal change in surface ocean pCO_2, and net sea-air CO_2 flux over the global oceans. *Deep Sea Research Part II: Topical Studies in Oceanography*, *56*, 554–577.

Taylor, J. R., & Ferrari, R. (2011a). Shutdown of turbulent convection as a new criterion for the onset of spring phytoplankton blooms. *Limnology and Oceanography*, *56*, 2293–2307.

Taylor, J. R., & Ferrari, R. (2011b). Ocean fronts trigger high latitude phytoplankton blooms. *Geophysical Research Letters*, *38*, L23601. https://doi.org/10.1029/2011GL049312

Townsend, D. W., Cammen, L. M., Holligan, P. M., Campbell, D. E., & Pettigrew, N. R. (1994). Causes and consequences of variability in the timing of spring phytoplankton blooms. *Deep-Sea Research Part I: Oceanographic Research Papers*, *41*, 747–765.

Venayagamoorthy, S. K., & Stretch, D. D. (2010). On the turbulent Prandtl number in homogeneous stably stratified turbulence. *Journal of Fluid Mechanics*, *644*, 359–369.

Whitt, D. B., Lévy, M., & Taylor, J. R. (2017). Low-frequency and high-frequency oscillatory winds synergistically enhance nutrient entrainment and phytoplankton at fronts. *Journal of Geophysical Research: Oceans*, *122*, 1016–1041. https://doi.org/10.1002/2016JC012400